Multifunctional Pd/Ni-Co Catalyst for Hydrogen Production by Chemical Looping Coupled Sorption Enhanced Steam Reforming of Acetic Acid

Javier Fermoso,[b] María V. Gil,[c] Fernando Rubiera[c] and De Chen*[a]

[a] Prof. D. Chen, Department of Chemical Engineering, *Norwegian University of Science and Technology, Sem Sælands vei 4, Trondheim 7491 (Norway)*
[b] *Dr. J. Fermoso, Thermochemical Processes Unit, IMDEA Energy Institute, Avenida Ramón de la Sagra 3, 28935 Móstoles (Spain)*
[c] *Dr. M. V. Gil, Dr. F. Rubiera, Instituto Nacional del Carbón, INCAR-CSIC, Apartado 73, 33080 Oviedo (Spain)*

Abstract

High yield of H_2 of high purity from acetic acid, a model compound of bio-oil from the biomass fast pyrolysis, was produced by sorption enhanced steam reforming (SESR). An oxygen carrier was introduced into a chemical loop (CL) coupled to the cyclical SESR process to supply heat in situ for the endothermic sorbent regeneration, in order to increase the energy efficiency of the process. A new multifunctional 1%Pd/20%Ni-20%Co catalyst was developed for use both as oxygen carrier in the CL and as reforming catalyst in the SESR, while a CaO-based material was used as CO_2 sorbent. In the sorbent air-regeneration step, the Ni-Co atoms in the catalyst undergo strong exothermic oxidation reactions which provide heat for the CaO decarbonation. The addition of Pd to the Ni-Co catalyst makes the catalyst active throughout the whole SESR-CL cycle. Pd significantly promotes the reduction of Ni-Co oxides to metallic Ni-Co during the reforming stage, which avoids the need for a reduction step after regeneration. H_2 yield above 90% and H_2 purity above 99.2 vol.% were obtained.

Introduction

Fossil fuels are currently the most important source of hydrogen production (96%). Production of pure hydrogen from the steam methane reforming (SMR) of natural gas is still the most commonly used process, representing 48% of the total production of hydrogen. However, it requires a multi-unit process configuration involving a high temperature and high pressure catalytic steam reformer, high and low temperature water-gas shift (WGS) reactors and a multi-column pressure swing adsorption (PSA) process to purify the H_2 produced. Over the next few decades, the demand for hydrogen is expected to grow exponentially, not only for conventional industrial uses but also for clean energy generation, particularly in fuel cell applications[1]. The generation of clean and efficient energy by fuel cells will require the production of very high-purity H_2 on a massive scale for use in transportation and stationary power systems[2]. Nevertheless, the full environmental benefit of applying hydrogen as a clean energy carrier can only be achieved if hydrogen is produced from renewable sources. There is growing interest in developing new technologies to produce hydrogen from renewable sources, such as biomass and water, by high-energy efficient, cost-competitive and environmentally-friendly means. The production of hydrogen from biomass could provide not only the hydrogen required in biomass refineries but also green hydrogen for use in oil refineries, which would offer a greener use of the conventional fossil fuels.

Several processes are currently being investigated for producing hydrogen from biomass-based compounds. Hydrogen can be generated from biomass by biological processes[3] and direct thermochemical processes, such as gasification[4], as well as by the reforming of biomass-derived oxygenates resulting from hydrolysis, fermentation, flash pyrolysis or gasification[5]. Fast or flash pyrolysis represents an attractive platform for producing pyrolysis oil (bio-oil) as a resource for hydrogen production through catalytic reforming[6]. It provides an interesting option for converting large-volume solid biomass materials to bio-oils, thereby reducing transportation costs. Bio-oil is a complex mixture of a large number of compounds, including aldehydes, alcohols, ketones and acids, as well as more complex carbohydrate- and lignin-derived oligomeric materials emulsified with water[7]. The aqueous phase contains some organic compounds such as acids, alcohols, aldehydes, ketones and sugars. Intensive research studies on the steam reforming of model compounds of bio-oil can be found in the literature, with the main focus on the development of efficient and stable catalysts[6a, 8]. Acetic acid is frequently chosen as a model compound[8-9] because it is one of the main constituents of the water soluble fraction of bio-oil[10]. A number of studies on the conventional steam reforming process of bio-oil compounds have been previously reported[6a, 8-9, 11]. However, the sorption enhanced reforming of bio-oil compounds for the production of highly pure hydrogen has not been explored.

Hydrogen production by sorption enhanced steam reforming (SESR) involves the introduction of a solid CO_2 sorbent, such as CaO, which is incorporated into the catalyst bed for the in situ removal of carbon dioxide from the gas phase. Thus, the equilibrium of steam reforming and WGS reactions is shifted towards hydrogen production, which increases the H_2 concentration in the gas produced while complete conversion can be almost achieved. One of the major challenges of the SESR process for improving energy efficiency is the high-temperature sorbent regeneration step, which is a highly endothermic reaction and requires a high heat input. Operating the sorption enhanced reforming process in a continuous mode can be achieved by using two interconnected circulating fluidized-bed reactors, a reformer/carbonator and a calciner, where the process involves the transport of solids (CO_2 sorbent and reforming catalyst) between them. The direct combustion of additional hydrocarbons such as methane or the oxidation of transition metals such as Ni, Co and Fe in the calciner reactor seems to be the most practical option for providing the necessary heat when a high temperature is needed in the process. The use of air to regenerate the sorbent presents certain advantages, such as its low cost in comparison with inert gases or steam. In addition, any coke that may form on the catalyst surface can be in turn burned off during the sorbent regeneration, which would regenerate the catalyst and partially provide heat for the endothermic decarbonation reaction. It is well known that rapid catalyst deactivation is one of the major obstacles in the SESR of bio-oil for hydrogen production. The presence of oxygen during the sorbent regeneration stage would cause oxidation of the reforming catalyst if a conventional nickel-based catalyst were used. The oxidized state of the metallic catalysts is known to be much less active than the reduced state. A thorough reduction treatment is therefore required between the regeneration step and the sorption enhanced steam reforming stage of the whole cycle.

Some novel reforming systems that use metal chemical loops (CL) have been proposed in the literature to solve the problem of the energy supply to perform the endothermic regeneration of the CO_2 sorbent in the SESR process[12]. In these processes, the heat generated by the exothermic metal oxidation reaction during the regeneration of the sorbent with air is supplied to the endothermic reaction of $CaCO_3$ decomposition. Fixed-bed reactors with alternating feedstreams of fuel/steam and air have also been considered to carry out

the SESR-CL process, where the bed consists of a mixture of the metal-based oxygen carrier and the CO_2 sorbent. These dynamically operated packed bed reactors take advantage of the high efficiency with which the heat is transferred from the metal particles oxidized with air to the $CaCO_3$ particles inside the same bed[13]. This represents a promising technology for the production of hydrogen by sorption enhanced reforming processes. However, the challenges involved in the development of multifunctional catalyst materials for obtaining high-purity H_2 by the SESR process have still not been addressed in the literature.

Furthermore, two features of the SESR process that are essential for obtaining high-purity hydrogen, namely low temperature (400-600 ºC) and high conversion, and in turn, a very low reactant concentration, require the use of very active reforming catalysts. The main requirements of the catalyst are a high activity and selectivity towards H_2 and CO formation, through the cleavage of C-C and C-H bonds, as well as a high catalytic activity for the high-temperature WGS reaction. The catalyst will also need to maintain a strong resistance to deactivation from sintering or coke formation. In addition, it will need to function efficiently as an oxygen carrier if a chemical loop is to be coupled to the SESR process. High reduction ability by the metals within the catalysts will also be required. Our previous studies have shown that a Ni-Co catalyst derived from hydrotalcite-like material (HT) is highly effective in the SESR process with several biomass-derived compounds, such as syngas[14], glycerol[5b, 15], ethanol[16] and glucose[17]. Nickel-based catalysts are generally used in hydrocarbon steam reforming due to their high catalytic activity. However, noble metals, such as Ru and Pd, can be introduced into the catalyst because of their higher resistance to carbon deposition[18]. In addition, Pd is expected to be less sensitive to oxidative treatments at high temperatures. Moreover, Pd has a high catalytic activity for the WGS reaction, which could enhance the production of H_2 by converting CO to CO_2, as another important criterion to be considered when selecting catalysts for sorption enhanced reforming processes[19].

In the present study, a new multifunctional Pd/Ni-Co catalyst derived from hydrotalcite-like materials (HT) has been developed as both oxygen carrier and reforming catalyst in the SESR of acetic acid coupled to a chemical looping process. The promotion of the Ni-Co catalyst with Pd was carried out for the purpose of eliminating the catalyst reduction after the air regeneration step in the SESR cyclic process, and in turn for enhancing the WGS reaction.

Hydrogen production by chemical looping coupled sorption enhanced reforming

During the steam reforming process with acetic acid [Eq. (1)], apart from H_2 and CO_2, CO and CH_4 are also expected to be generated in large quantities due to thermodynamic equilibrium limitations and complex reaction pathways, including thermal decomposition, which might also lead to the formation of intermediates and coke.

$$C_2H_4O_2 + 2H_2O \rightarrow 4H_2 + 2CO_2;\ \Delta H_r^0 = +183.7\ kJ\ mol^{-1} \quad (1)$$

The incorporation of a CO_2 sorbent, such as CaO, in the catalyst bed removes CO_2 in situ from the gas phase, as illustrated in Equation (2).

$$CaO_{(s)} + CO_2 \leftrightarrow CaCO_{3(s)};\ \Delta H_r^0 = -177.8\ kJ\ mol^{-1} \quad (2)$$

Due to the equilibrium shift effect, the reduction of CO_2 concentratio in gas phase promotes the water-gas shift (WGS) reaction [Eq. (3)], and in turn the CH_4 reforming reaction [Eq. (4)].

$$CO + H_2O \leftrightarrow H_2 + CO_2;\ \Delta H_r^0 = -41.2\ kJ\ mol^{-1} \quad (3)$$

$$CH_4 + H_2O \leftrightarrow 3H_2 + CO;\ \Delta H_r^0 = +206.2\ kJ\ mol^{-1} \quad (4)$$

As a result, the CO and CH_4 contents are significantly reduced, and the hydrogen concentration in the product gas is increased. The global process involved is the sorption enhanced steam reforming (SESR), whose overall reaction is represented by Equation (5).

$$C_2H_4O_2 + 2H_2O + 2CaO_{(s)} \rightarrow 4H_2 + 2CaCO_{3(s)};\ \Delta H_r^0 = -172.0\ kJ\ mol^{-1} \quad (5)$$

Sorbent regeneration takes place via the endothermic decarbonation of the $CaCO_3$ generated during the reforming stage to produce CO_2 and CaO again [reverse of Eq. (2)]. The decarbonation reaction is obtained by reducing the partial pressure of CO_2 in the gas phase to below the CaO-$CaCO_3$ equilibrium value, which is a function of the temperature. This is commonly achieved by increasing the temperature, and hence the equilibrium pressure. The use of air for sorbent regeneration lowers the CO_2 partial pressure due to its dilution with N_2, which will allow a lower temperature to be used for decarbonation. However, if a highly-concentrated CO_2 regeneration stream is required for CO_2 storage or other purposes, calcination needs to be carried out under oxy-fuel combustion conditions (in a CO_2-rich atmosphere) to avoid higher process costs due to the dilution of CO_2 with nitrogen[20].

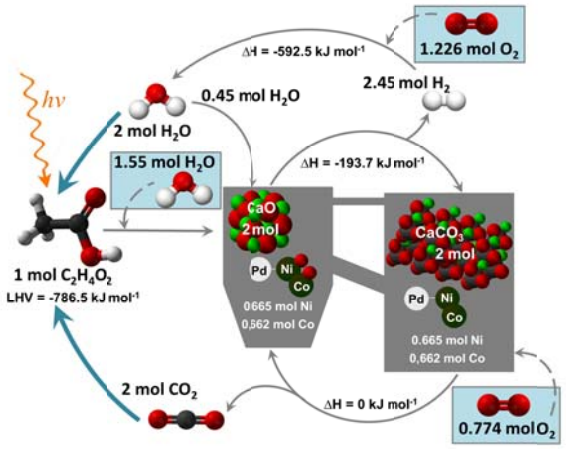

Figure 1. Assembled SESR-CL process. CaO is used as CO_2 sorbent and Pd/Ni-Co HT as both oxygen carrier and reforming catalyst.

Figure 1 shows a general scheme of the assembled SESR-CL process used in the present study. It consists of two steps: sorption-enhanced steam reforming (SESR) and sorbent regeneration (REG), where Pd/Ni-Co HT is used as both the reforming catalyst and oxygen carrier and CaO is employed as CO_2 sorbent. During the SESR stage, a H_2-rich stream is produced by the sorption enhanced steam reforming of acetic acid, with the simultaneous carbonation of CaO by the CO_2 produced from the reforming reaction.

In the REG stage, the calcination of the $CaCO_3$ formed in the previous step takes place while at the same time the oxidation of the Ni and Co metals by oxygen occurs according to Equations (6) and (7) to form oxides. These reactions provide in situ heat which can be used for regenerating the sorbent [reverse of Eq. (2)].

$$Ni_{(s)} + 1/2O_2 \rightarrow NiO_{(s)};\ \Delta H_r^0 = -244.3\ kJ\ mol^{-1} \quad (6)$$

$$Co_{(s)} + 2/3O_2 \rightarrow 1/3Co_3O_{4(s)};\ \Delta H_r^0 = -292.88\ kJ\ mol^{-1} \quad (7)$$

The reduction of the metal oxides will proceed during the subsequent SESR stage via the consumption of part of the H_2 produced. Ni and Co metallic phases are again formed as shown in Equations (8) and (9).

$$NiO_{(s)} + H_2 \rightarrow Ni_{(s)} + H_2O;\ \Delta H_r^0 = +2.51\ kJ\ mol^{-1} \quad (8)$$

$$Co_3O_{4(s)} + 4H_2 \rightarrow 3Co_{(s)} + 4H_2O;\ \Delta H_r^0 = -88.70\ kJ\ mol^{-1} \quad (9)$$

The oxidation and reduction steps of the Ni and Co metals comprise a chemical loop, which is coupled to the SESR process. The exothermic oxidation of the metals would be used to obtain part of the heat needed for the decarbonization of the previously formed $CaCO_3$. The in-situ heat supply thereby reducing the energy consumption of the overall process by reducing the energy loss using external heat supply. Energy efficiency estimation for the studied SESR-CL process lies outside the scope of this paper, but it has been demonstrated in similar chemical looping processes[12b] that there is a great potential for achieving a high degree of energy efficiency with this type of process. A brief energy balance of the whole process has been carried out on a base of 1 mole of $C_2H_4O_2$, as it is shown in Figure 1. Following the reaction stoichiometry Equation (5), 374.4 g (2 mole of CaO) uncalcined dolomite (98.5% $CaMg(CO_3)_2$) are needed in the process. For an autothermal regeneration process, 195.2 g of reduced catalyst (0.665 mole of Ni and 0.662 mole of Co) per mole of $C_2H_4O_2$ would be required. However, during the reforming stage, the reduction of the catalyst metals will consume a part of the produced H_2 and 2.45 mole of H_2 will be produced per mole of $C_2H_4O_2$ (Figure 1).

In the present work, the effect of promotion of Pd to the Ni-Co HT catalyst was investigated in a comparative study of the SESR of acetic acid carried out using both reduced and oxidized Pd/Ni-Co catalysts, as well as reduced and oxidized Ni-Co catalysts, upon catalyst activity and hydrogen purity. The production of high-purity hydrogen by the sorption enhanced reforming of acetic acid when coupled to a chemical loop was tested experimentally. The effects of the operation conditions on hydrogen production were also studied.

Results and Discussion

Catalyst characterization

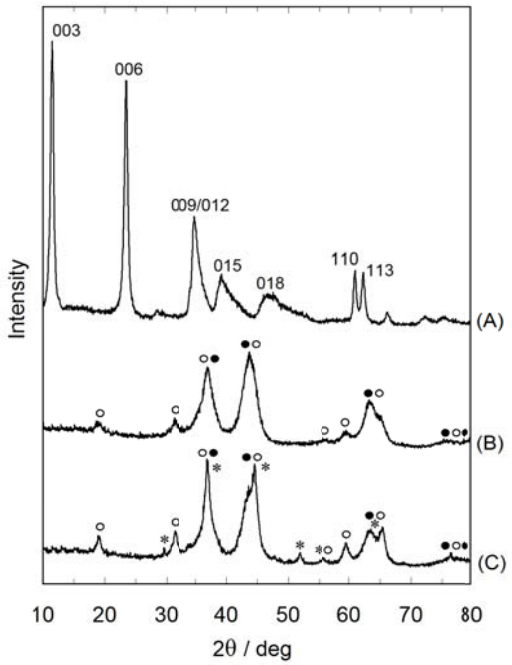

Figure 2. X-ray diffraction (XRD) patterns of uncalcined Ni-Co HT (A), calcined Ni-Co HT (B) and calcined Pd/Ni-Co (C). Peaks marked with (●) are characteristic of NiO, $NiMgO_2$ and MgO; peaks marked with (○) are characteristic of Co_3O_4, $NiCo_2O_4$, $CoAl_2O_4$, Co_2AlO_4, $MgCo_2O_4$, $NiAl_2O_4$ and $MgAl_2O_4$; and peaks marked with (*) are characteristic of $PdCoO_2$.

Figure 2 shows the powder X-ray diffraction patterns of the uncalcined Ni-Co HT (A); calcined Ni-Co HT (B); and calcined Pd/Ni-Co HT (C). Figure 2 A shows that the hydrotalcite-like material was successfully synthesized since the observed diffraction reflections correspond to a typical crystalline structure of hydrotalcite-like materials. This structure exhibits sharp and symmetric diffraction peaks for the (003), (006), (009), (110) and (113) crystal planes and broad and asymmetric peaks for the (012), (015) and (018) planes, which are characteristic of the double sheet hydroxide structures of hydrotalcite-like materials[21].

When a hydrotalcite-like material is treated at high temperatures, it loses its structure and the material becomes a mixture of oxides, mixed oxides and spinels. Figures 2 B and 3 C show the XRD patterns of the calcined HT samples. It can be seen that, after calcination at 600 ºC, reflections typical of a HT structure disappear and those related to mixed metal oxides are observed. The CoO and Co_2O_3 single oxides were not identified in the XRD patterns, indicating that Co cations were located in Co_3O_4 or $NiCo_2O_4$ oxides and in spinel-like structures, such as $CoAl_2O_4$, Co_2AlO_4 and $MgCo_2O_4$. These phases, together with $NiAl_2O_4$ and $MgAl_2O_4$ spinels, have very similar characteristic XRD patterns[22], as reflected by the severe overlapping in the XRD patterns of the calcined HT samples. Complex overlapping is also observed in the case of the NiO, $NiMgO_2$ and MgO phases, which have similar reflection angles. In general, it is difficult to discern from the XRD patterns of the calcined HT, whether nickel and cobalt ions have been incorporated into the alumina and magnesia spinel or if they have been mixed separately with the solid solution of the matrix. Furthermore, the

XRD pattern of the calcined Pd/Ni-Co HT, Figure 2 C, shows that peaks corresponding to $PdCoO_2$ can be seen at 2θ of 30º and 52º. Other peaks corresponding to palladium oxide may be overlapping at ca. 2θ of 38º, 42º, 56º and 65º.

The main properties of the prepared catalysts are presented in Table 1. The uncalcined Ni-Co HT precursor shows a BET surface area of 115 $m^2\ g^{-1}$. The average pore size of 15 nm suggests that the catalyst is a mesoporous material. After calcination at 600 ºC, the calcined Ni-Co HT catalyst experienced an increase in surface area to 187 $m^2\ g^{-1}$. This is in good agreement with the results of Bellotto et al.[23] who studied the evolution of the surface area of HTs during their decomposition and found that an increase in the surface area had occurred mainly due to the breakdown of the initial HT sheet structure. After the impregnation of Pd, i.e., the calcined Pd/Ni-Co HT catalyst, the surface area decreased to 144 $m^2\ g^{-1}$. The loss of BET area and pore volume can be attributed to the deposition of Pd-species in the pores.

Table 1. Physical-chemical properties of the HT-derived catalysts.

Catalyst	BET			Chemisorption		
	surface area $[m^2\ g^{-1}]$	pore volume $[cm^3\ g^{-1}]$	pore diameter [nm]	D[a] [%]	d [nm]	metal surface area $[m_{metal}^2\ g_{cat.}^{-1}]$
uncalcined Ni–Co HT	115	0.52	15	8.0	12	21
calcined Ni–Co HT	187	0.80	14	11.3	9	30
calcined Pd/Ni–Co HT	144	0.52	12	7.8	13	21

[a] The dispersion of metals was measured on reduced samples.

Chemisorption of hydrogen on the reduced catalyst was used to estimate the metal dispersion and particle size (Table 1). The dispersion was slightly higher on the calcined Ni-Co HT catalyst than on the uncalcined one, resulting in smaller crystals and a higher metal surface area. When Pd was added to the catalyst, dispersion, crystal size and the metal surface area showed similar values to those of the uncalcined Ni-Co HT catalyst. The values were similar to those of the Ni-Co hydrotalcite-like catalyst used in previous experiments[24].

TPR profiles of the calcined Ni-Co and calcined Pd/Ni-Co HT-derived catalysts are shown in Figure 3. Both samples displayed two reduction regions. However, upon the addition of palladium to the catalyst, a shift of the reduction peaks towards lower temperatures was observed, indicating that the Pd accelerated the reduction of the Ni-Co catalysts.

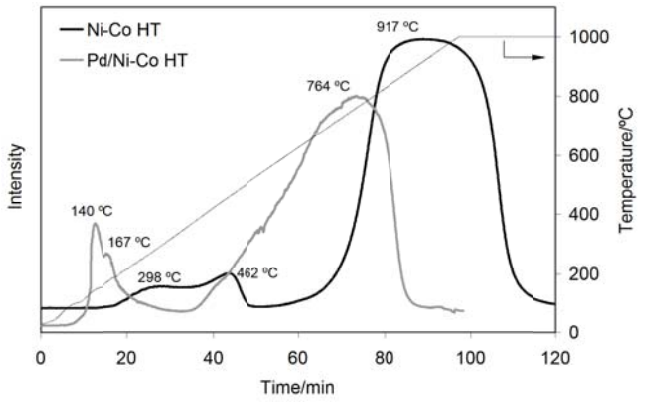

Figure 3. Temperature programmed reduction (TPR) profiles of the calcined HT-derived catalysts.

In previous studies, it was demonstrated that the reducibility of Ni and Co was affected by the amount of the metal ions initially substituted into the HT lattice during the preparation, and the reduction peak is generally assigned to the transfer of metal atoms from the bulk solid solution to the surface[25]. He et al.[24] investigated Ni-Co HT catalysts with different metal compositions and deduced that Co^{2+} ions were more difficult to substitute into the HT structures than Ni^{2+} ions, which caused only a fraction of the Co ions to be deeply incorporated within the HT-derived matrix, some of them tending to be dispelled towards the surface. During the reduction, this led to differences in the extraction of Co ions from the HT-derived matrix, giving rise to two reduction regions: 200-500 ºC corresponding to the easily reducible Co ions and 620-920 ºC corresponding to the remaining Co/Ni ions. The same profile was also obtained in the present study for the Ni-Co HT-derived catalyst. Li et al.[26] detected in Co-based HT catalysts a low temperature peak between 275-455 ºC which they attributed to the reduction of Co_3O_4 to CoO, in agreement with our findings. Muñoz et al.[27] pointed out that signals in the low-temperature zone (<350 ºC) in the TPR profiles of Ni-Co hydrotalcite-like catalysts corresponded to the reduction of Co_3O_4 species to CoO and Co, whereas a second low-temperature event (350-550 ºC) was attributed to the complex surface reduction of the octahedral Co^{2+}/Co^{3+} species contained in Co_2AlO_4 and/or $CoAl_2O_4$ structures and to the reduction of NiO species.

As mentioned above, both reduction regions were shifted to lower temperatures in the case of the Pd/Ni-Co HT-derived catalyst. Melo and Morlanés[18] also reported that in a HT-derived catalyst produced by co-precipitation, Pd was reduced at much lower temperatures than Ni and Co and that it could even be partially reduced at room temperature, indicating that the interaction of the element with the support was much weaker. Li et al.[26] also observed that the reduction peaks of the Co-based HT catalysts were markedly shifted to lower temperatures after the incorporation of Pd, indicating that the reduction of Co oxide had been facilitated significantly by the introduction of Pd into the HT structure, due to the fact that the palladium catalyzed the cobalt oxide reduction. Conner and Falconer[28] demonstrated that the reduction temperature of several metal oxides (CuO, NiO, Co_3O_4) by H_2 could be lowered by the addition of transition metals, Pt and Pd being the most efficient ones. According to Jacobs et al.[29] the addition of small amounts of noble metal promoters, such as Pt, Pd and Ru, to cobalt over alumina, can be employed to facilitate catalyst reducibility, since the promoter would be reduced first and it could then catalyze the reduction of cobalt oxide, thereby shifting the reduction temperature of both steps ($Co_3O_4 \rightarrow CoO$ and $CoO \rightarrow Co$) to lower values. These authors suggested that a fraction of the promoter atoms are positioned at the edge of the cobalt clusters, where reduction can affect the

promoter first. The adsorbed hydrogen would be firstly dissociated on the previously reduced noble metal atoms and converted to active hydrogen, which could migrate to the neighboring cobalt oxide clusters and catalyze the reduction of the cobalt oxides. In short, hydrogen spillover from the reduced Pd metal would facilitate the reduction of the cobalt oxides and significantly increase the reducibility of Pd-promoted catalyst. Metal oxides are reduced more rapidly in the presence of transition metals because the oxides themselves are not capable of dissociating H_2 at a significant rate at the same temperatures where transition metals readily dissociate H_2[28]. In conclusion, Pd had a clear promoting effect on the reduction of nickel and cobalt oxides.

The reduced-passivated Pd/Ni-Co HT catalyst was subjected to SEM analysis. Figure 4 shows the SEM image and complementary EDS elemental mapping of the Pd-promoted catalyst. In Figure 4 a, it can be seen that Ni and Co have similar distributions, indicating the homogeneous mixing of both elements in the metal particles and suggesting that an alloy has been formed. Furthermore, the incipient wetness impregnation method resulted in a good distribution of palladium on the catalyst particles, as is shown in Figure 4 a. EDS microanalysis (Figure 4 b) confirms that the catalyst composition was approximately as expected.

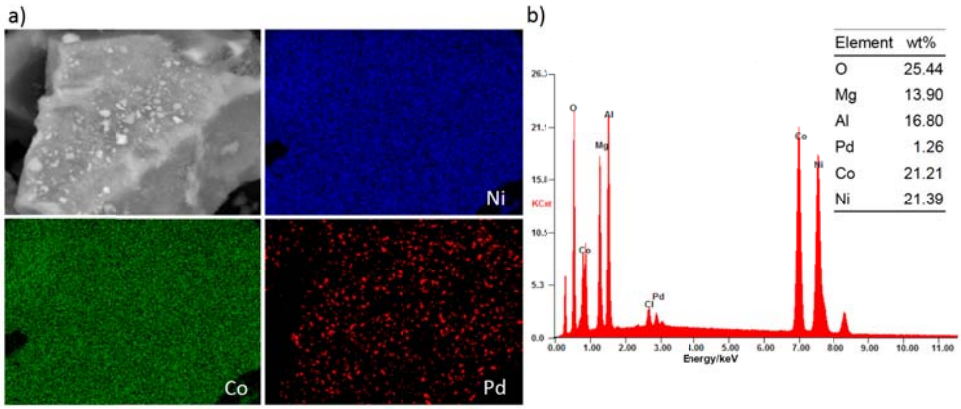

Figure 4. SEM image and EDS elemental mapping of Ni, Co and Pd (a); and EDX microanalysis (b) of the Pd/Ni-Co HT catalyst.

Effect of the state of the active metal in the catalyst on SESR activity

The catalytic activity of the Ni-Co HT and Pd/Ni-Co HT catalysts was tested under SESR conditions using acetic acid as a bio-oil model compound and calcined dolomite as CO_2 sorbent. The experiments were performed at 575 ºC and 1 atm, with a molar steam-to-carbon ratio of 3 and a liquid flow rate of 2.5 g h^{-1} (WHSV = 0.89 h^{-1}), following the experimental procedure described in the Experimental Section. The H_2 yield and the dry gas composition after the SESR process were evaluated using both the reduced and unreduced (i.e., oxidized) catalysts. After the air regeneration step, the regenerated catalyst was used directly in the SESR experiments in the case of the 'unreduced catalyst', whilst the reduction step described in the experimental procedure was carried out after regeneration and before the SESR process in the case of the 'reduced catalyst'. The effect of the addition of Pd to the catalyst composition was also analyzed by comparing the results obtained for the Ni-Co HT and Pd/Ni-Co HT catalysts.

Figure 5 shows the evolution of the gas composition (N_2 free and dry basis) as a function of time during the SESR experiments of acetic acid, whereas Figure 6 shows the H_2 yield as a function of time on stream. As has been reported in previous studies during the SESR of different biomass-derived compounds[4b, 5b, 15-16], the evolution of the gas effluent composition in a sorption enhanced process can be typically divided into three stages: pre-breakthrough, breakthrough and post-breakthrough. During the pre-breakthrough stage, the CO_2 sorbent effectively captures CO_2. At the same time, the reforming reaction is shifted towards the product side by the removal of CO_2 and the concentration of H_2 increases, whereas the CO and CH_4 concentrations are very low. In the breakthrough region, the CaO sorbent becomes saturated, which is reflected by a rapid rise in the CO_2 concentration and a reduction in the hydrogen content. In the post-breakthrough region, CO_2 capture by the sorbent is negligible and conventional steam reforming is assumed to occur. As is shown in Figure 5 d, the CO_2 evolution profile during the pre-breakthrough stage is similar for both catalysts in both the reduced and unreduced states. This indicates that the CaO-CO_2 reaction was not affected either by the state of the catalyst or by the reforming reactions kinetics and that all the CO_2 produced reacted with the sorbent until saturation.

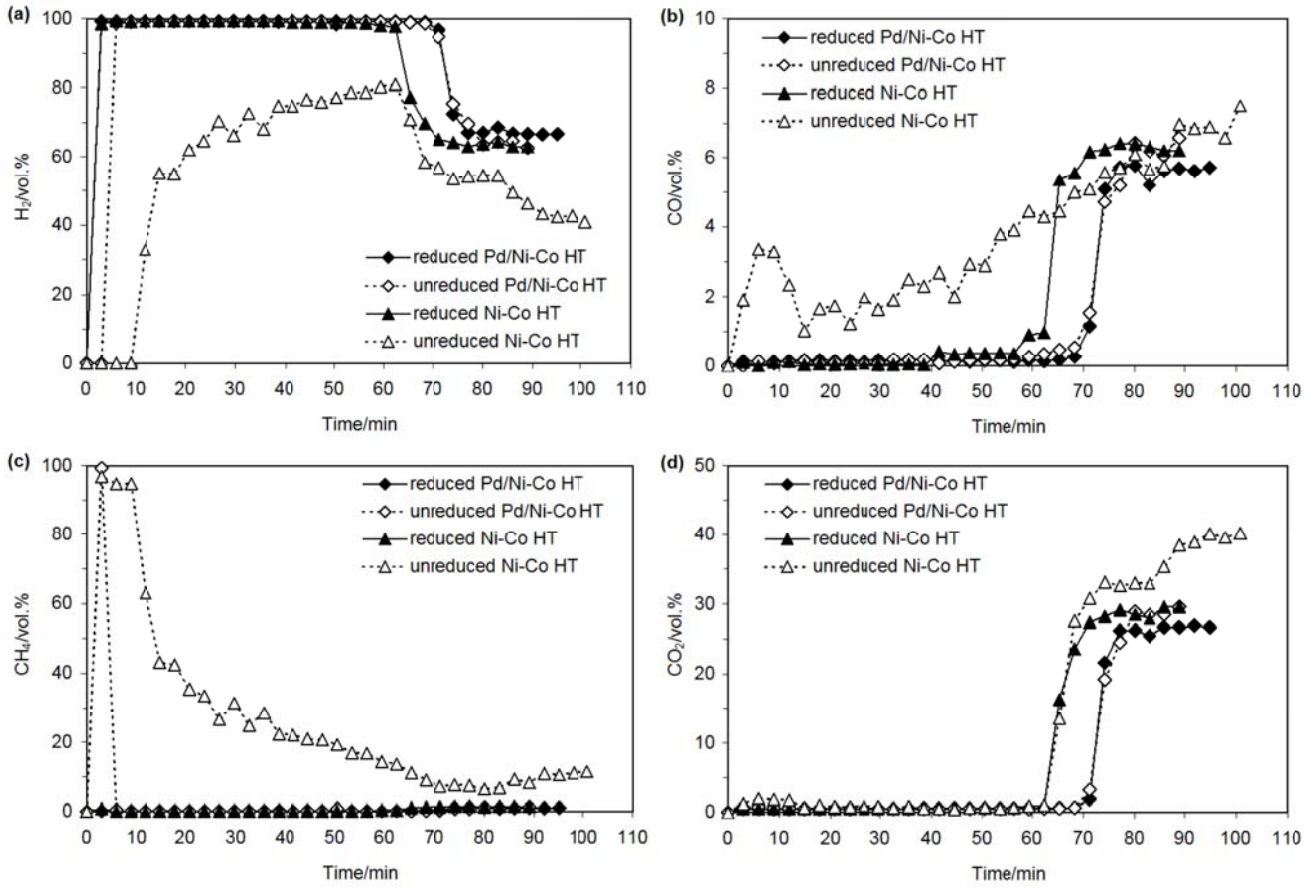

Figure 5. Evolution of the product gas composition (N_2 free and dry basis) with time on stream during the SESR process of acetic acid using different catalysts: (a) H_2, (b) CO, (c) CH_4 and (d) CO_2. Reaction conditions: 575 ºC; 1 atm; steam/C = 3 mol/mol; WHSV = 0.89 h^{-1}; sorbent to catalyst = 5 g/g and calcined dolomite as sorbent.

In general, the steady-state H_2 yield (Figure 6), as well as H_2, CO and CH_4 concentrations in the gas effluent during the pre-breakthrough stage (Figure 5) were similar for all the studied catalysts, except for the

case of the unreduced Ni-Co HT. For this catalyst, a much lower H_2 yield and H_2 purity, and higher CO and CH_4 contents in the gas effluent, were observed from the beginning of the experiment during the course of the SESR reactions. In this case, the steady-state phase was difficult to reach. When this catalyst had been subjected to reduction after regeneration and prior to the SESR experiment, i.e., the reduced Ni-Co HT, a higher H_2 concentration was observed from the beginning of the experiment (99.17%), as can be seen in Figure 5 a, together with much lower contents of CO and CH_4 in the effluent gas (Figures 5 b and 5 c, respectively). With the use of the reduced Ni-Co HT catalyst, the H_2 yield quickly increased to a much higher value (90.84%), as Figure 6 shows. These results indicate that Ni and Co oxides are not very active in either reforming reactions (acetic acid and/or hydrocarbons derived from its thermal decomposition) or in WGS. In addition, most of H_2 produced from the beginning of the experiment would be consumed in reducing the Ni and Co oxides in the unreduced Ni-Co HT catalyst. Consequently, the H_2 yield (Figure 6) and H_2 purity (Figure 5 a) with the unreduced Ni-Co HT catalyst slowly increased with time, whereas the CH_4 and CO contents decreased significantly (Figures 5 c and 5 b, respectively).

It can therefore be concluded that, after sorbent regeneration under an air atmosphere, the reduction of the Ni-Co HT catalyst must be carried out before the SESR process in order to obtain a high degree of hydrogen purity and a high yield. Dupont et al.[12c] carried out the reforming of methane and sunflower oil with in situ CO_2 capture using a Ni-based material as oxygen carrier. They observed an initial 'dead time' where no H_2 was evolved during the reforming stage when the catalyst had not been previously reduced. They then concluded that a catalyst reduction step had to be carried out before the SESR process since the reforming reactions only proceeded once sufficient NiO in the oxygen carrier had been reduced back to Ni.

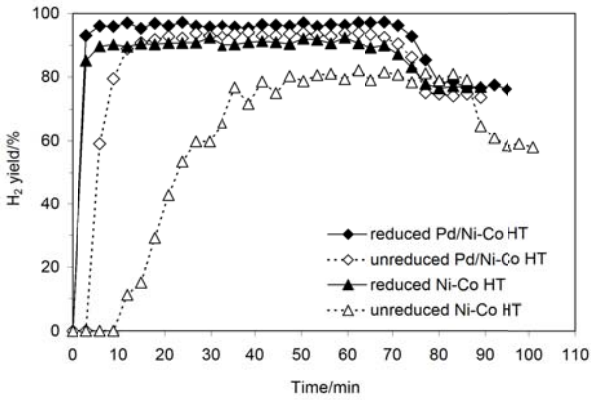

Figure 6. Evolution of the H_2 yield with time on stream during the SESR process of acetic acid using different catalysts. Reaction conditions: 575 ºC; 1 atm; steam/C = 3 mol/mol; WHSV = 0.89 h^{-1}; sorbent to catalyst = 5 g/g and calcined dolomite as sorbent.

In the case of the Pd-promoted catalysts, when the reduced and unreduced Pd/Ni-Co HT catalysts are compared, a difference in the H_2 yield results (96.24% and 92.20% respectively) is also observed, but it is much less marked than in the case of the Ni-Co HT catalyst (Figure 6). The steady-state H_2 concentrations in the effluent gas during the pre-breakthrough stage were quite similar for both the reduced and unreduced Pd-catalysts (99.24 and 99.15%, respectively), as Figure 5 a shows, which also occurs with the CO and CH_4 concentrations. When the unreduced Pd/Ni-Co HT catalyst was used, an initial short delay in reaching the

maximum H_2 concentration and H_2 yield values was detected. The short period of hydrogen breakthrough suggests that the rapid reduction of Pd/Ni-Co oxides occurred in the initial stage, where no formation of methane or CO was detected. During the oxidation process at 770 ºC, metallic Ni and Co can be expected to undergo oxidation[30], but metallic Pd possibly does not suffer oxidation. It has been demonstrated that PdO could be decomposed to Pd at 680-810 ºC and reformed at much lower temperatures, 470-730 ºC, depending on the support material[31]. In the present work, it can be expected therefore that metallic Pd would not be oxidized during air regeneration at 770 ºC. The results in Figures 5 and 6 suggest that the unreduced Pd/Ni-Co catalyst, or Pd, is active in the reforming of acetic acid for producing hydrogen. The produced hydrogen then reduces the Ni-Co oxides to the active metal phases with only a short delay in the establishment of the steady-state SESR process. It can be concluded that the effects of the addition of Pd to the Ni-Co HT catalyst are two-fold in that it provides the initial reforming activity and enhances the reduction of Ni-Co oxides. This is borne out by the results of the TPR experiments (Figure 3). Dupont et al.[12c] in their experiments on the reforming of methane, first assumed that the reduction of the metal oxide (NiO) occurred via the reaction of the fuel with the metal oxide, i.e., by the combustion of the fuel without any direct contact with an oxygen-containing stream. However, they found that the metal oxide reduction reaction occurred preferentially via H_2 over CH_4. In the present study it can therefore be deduced that the in situ produced H_2 would reduce the oxidized Ni-Co phases in the catalyst.

According to the results of the present work, after the sorbent regeneration stage under an air atmosphere, it may be possible to eliminate the pre-reduction step before SESR process from the multi-step operation, and still achieve high H_2 purity and considerable H_2 yield values, by using Pd-promotion of the catalysts. In addition, the dolomite sorbent can be regenerated at 770 ºC in air, where the oxidation of Ni and Co can be expected to supply in situ heat for its regeneration. This suggests that a chemical loop between the metal and oxide forms of the Ni and Co in the unreduced catalyst is viable to occur during the cyclic SESR process. The multifunctional Pd/Ni-Co HT catalyst is shown as a promising material for use in the assembled SESR-CL cyclic process both as reforming catalyst and oxygen carrier, allowing a continuous cycling operation in fixed-bed reactors or solid circulating fluidized-bed reactors without the need for a catalyst reduction step between the air-regeneration and reforming stages.

Finally, if the results from the reduced Ni-Co HT and the reduced Pd/Ni-Co HT catalysts are compared, no significant differences in the gas composition during the steady-state SESR experiment are observed (Figure 5). However, there is a significantly higher H_2 yield in the case of the reduced Pd-promoted HT catalyst compared to the reduced Ni-Co HT, 96.24% and 90.84%, respectively (Figure 6). This highlights the beneficial effect of adding Pd to the catalyst on the H_2 yield, even in the case of the unreduced Pd-promoted HT catalyst (H_2 yield = 92.20%). However, it should be mentioned that the Pd/Ni-Co HT catalyst used in the present work has not been optimized. The Pd loading needs to be evaluated and optimized in future studies. The present work has focused on elucidating the role of Pd in the novel hydrogen production process that is proposed. Additional studies on the stability of the catalyst are currently being carried out using the Pd catalyst developed in the present study. Thus, the Pd-promoted catalyst is being applied with success to produce hydrogen using glycerol as feedstock in a similar process and preliminary results seem to indicate that the catalyst can be able to remain stable over 20 cycles of SESR.

Effect of space velocity on SESR activity

The study of the space velocity (WHSV) effect on the SESR of acetic acid was carried out at values of 0.89-17.86 h^{-1} (liquid flow rate of 2.5-50 g h^{-1}) in order to elucidate the effects of Pd on catalyst activity. The experiments were performed at 575 ºC, 1 atm and at a steam/C ratio of 3, following the experimental procedure described in the Experimental Section. The H_2 yield and the dry gas composition after the SESR process were evaluated using reduced Pd/Ni-Co HT, unreduced Pd/Ni-Co HT and reduced Ni-Co HT catalysts. Figure 7 shows the gas composition (N_2 free and dry basis) as a function of the WHSV during the SESR experiments with acetic acid. The effect of the space velocity on H_2 yield is shown in Figure 8. Hydrogen production by SESR involves several reactions, such as the reforming of acetic acid, a side reaction leading to methane formation and its reforming, as well as the water gas shift reaction. The catalyst activity on these reactions was evaluated at a high WHSV of 17.86 h^{-1}, where the H_2 yield and H_2 purity were much lower and the CO, CH_4 and CO_2 contents were much higher than at smaller WHSV values. The H_2 yield and purity values followed the following order: reduced Pd/Ni-Co HT > unreduced Pd/Ni-Co HT > reduced Ni-Co HT catalysts, while the CO and CH_4 contents followed the opposite order. This confirms that the unreduced Pd/Ni-Co HT catalyst is active in the reforming reaction. Although its activity is slightly lower than that of the reduced Pd/Ni-Co HT, it is higher than that of the reduced Ni-Co HT catalyst. When WHSVs of less than 3 h^{-1} were used, the gas compositions were rather close to the equilibrium values. However, whereas the H_2 yield and H_2 purity decreased, the CO, CH_4 and CO_2 contents increased slightly with increasing WHSV (Figure 7).

It can therefore be concluded that a low WHSV value of 0.89 h^{-1} is the most favorable for the SESR process of acetic acid under the conditions studied. Moreover, the effect of the space velocity on H_2 yield was much more significant than on the gas composition. The H_2 yield decreased from 96.24% to 83.00% when the WHSV increased from 0.89 h^{-1} to 2.68 h^{-1} for the reduced Pd/Ni-Co HT catalyst (Figure 8). The same trend in relation to the space velocity was observed for the unreduced Pd/Ni-Co HT, although the maximum values obtained were slightly lower than for the reduced Pd-promoted catalyst. The SESR of acetic acid at 575 ºC, 1 atm, steam/C of 3 and WHSV of 0.89 h^{-1} using the unreduced Pd/Ni-Co HT catalyst produced a H_2 yield equal to 92.20% and a H_2 purity of 99.15 vol.%.

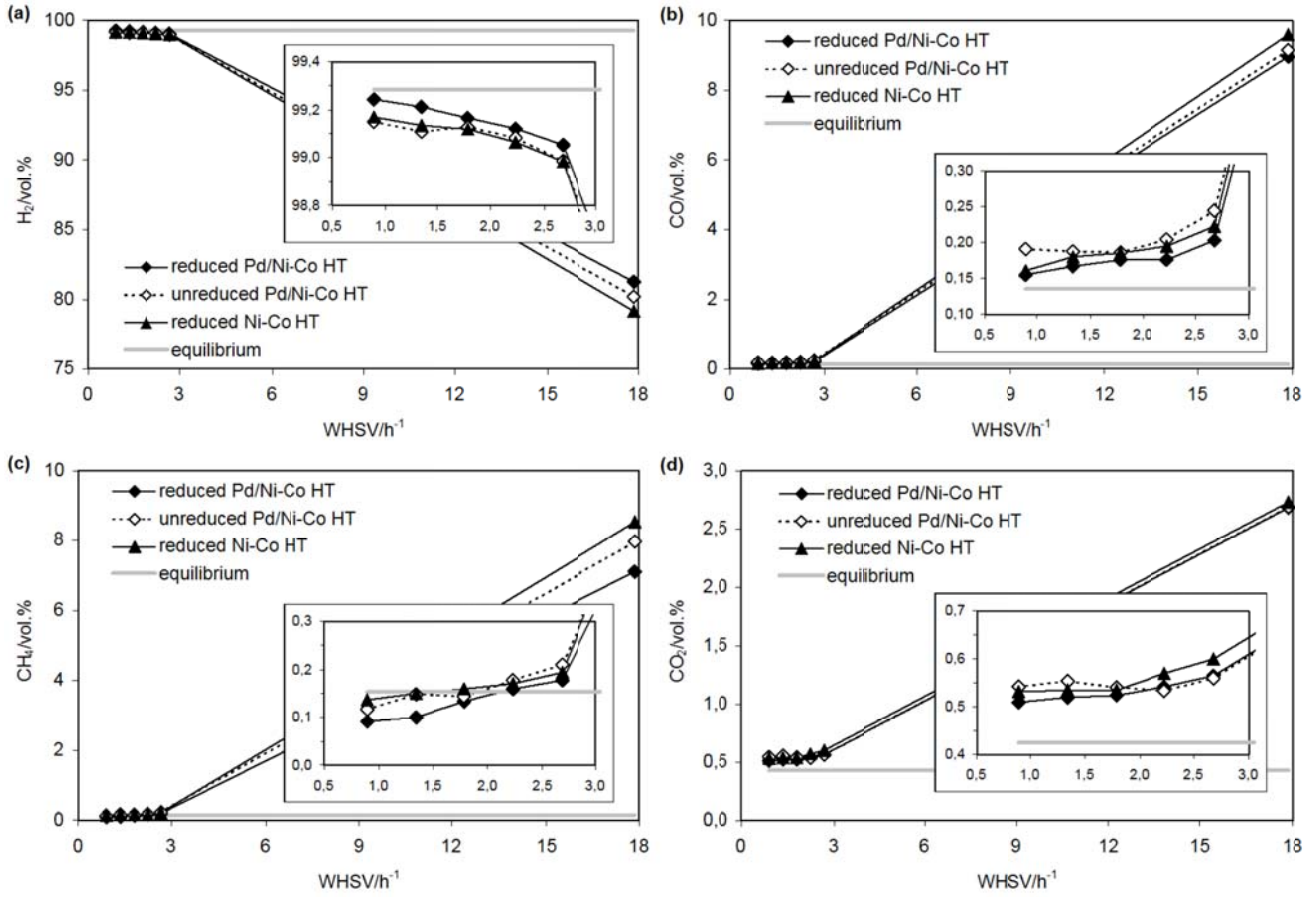

Figure 7. Effect of the space velocity (WHSV) on the product gas composition (N_2 free and dry basis) during the SESR process of acetic acid using different catalysts: (a) H_2, (b) CO, (c) CH_4 and (d) CO_2. Reaction conditions: 575 ºC; 1 atm; steam/C = 3 mol/mol; sorbent to catalyst = 5 g/g and calcined dolomite as sorbent.

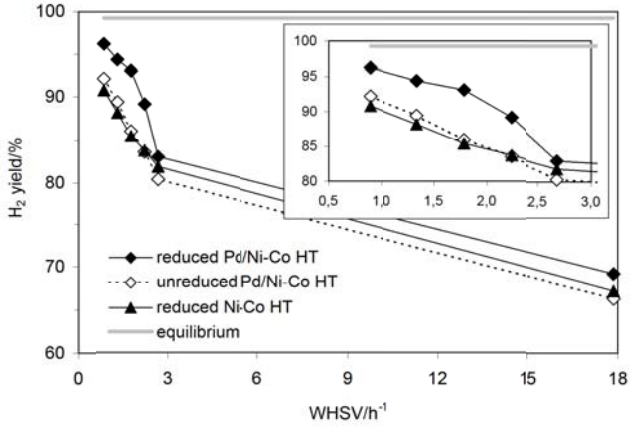

Figure 8. Effect of the space velocity (WHSV) on the H_2 yield during the SESR process of acetic acid using different catalysts. Reaction conditions: 575 ºC; 1 atm; steam/C = 3 mol/mol; sorbent to catalyst = 5 g/g and calcined dolomite as sorbent.

Effect of temperature on SESR activity

The study of the effect of temperature on the SESR of acetic acid was carried out between 475-625 ºC. The experiments were performed at 1 atm, a steam/C of 3 and a WHSV of 0.89 h^{-1} (liquid flow rate of 2.5 g h^{-1}), following the experimental procedure described in the Experimental Section. The H_2 yield and the dry gas composition after the SESR process were evaluated using reduced Pd/Ni-Co HT, unreduced Pd/Ni-Co HT and reduced Ni-Co HT catalysts. Figure 9 shows the gas composition (N_2 free and dry basis) as a function of the reaction temperature during the SESR experiments with acetic acid. The effect of the temperature on the H_2 yield is shown in Figure 10. The results indicate that as the temperature increased, the H_2 yield, and the CO and CO_2 contents also increased, whereas H_2 purity and CH_4 content decreased. A temperature of 650 ºC during the SESR process with acetic acid caused a significant decrease in H_2 purity, as well as a significant increase in the CO and CO_2 contents. The highest H_2 purity (99.81 vol.%) was obtained at 475 ºC for the reduced Pd/Ni-Co HT catalyst, but values higher than 99 vol.% were obtained for all the catalysts at temperatures below 575 ºC, as can be seen in Figure 9 a. The hydrogen content at temperatures below 575 ºC was very close to the thermodynamic equilibrium value for all the catalysts, but especially in the case of the reduced Pd/Ni-Co HT catalyst. The same trend was observed for the CO and CO_2 contents. With the unreduced Pd/Ni-Co HT catalyst, the SESR of acetic acid at 475 ºC also produced a high H_2 purity (99.70 vol.%).

As can be seen in Figure 9 b, the CO concentration decreased with decreasing temperature due to the favorable thermodynamics of the WGS reaction at low temperatures. The CO_2 concentration also decreased with decreasing temperature (Figure 9 d) because of the favorable thermodynamics of the carbonation reaction at low temperature. This led to a very weak sorption enhancement at 625 ºC, reflected in a very high CO_2 concentration under these conditions. Furthermore, since the CO_2 sorption led to an enhanced H_2 production by shifting the equilibrium of the steam reforming and water-gas shift reactions, a very low H_2 purity (Figure 9 a) and high CO concentration (Figure 9 b) were observed at high temperature conditions. In relation to the CH_4 content (Figure 9 c), it should be noted that the highest values were obtained at low temperatures (475 and 525 ºC) with the reduced Ni-Co HT catalyst, followed by the unreduced Pd-promoted catalyst and then by the reduced Pd-promoted one, showing the beneficial effect of the addition of Pd on the suppression of CH_4. High CH_4 contents are undesirable for hydrogen production because the CH_4 formation reactions consume hydrogen in the system, which makes it necessary to use a highly selective catalyst to suppress the methanation reaction during the SESR process. With increasing temperature, the shift of the methanation reaction to steam methane reforming produced very low CH_4 concentrations, indicating that the catalysts used effectively catalyzed the methane steam reforming reaction.

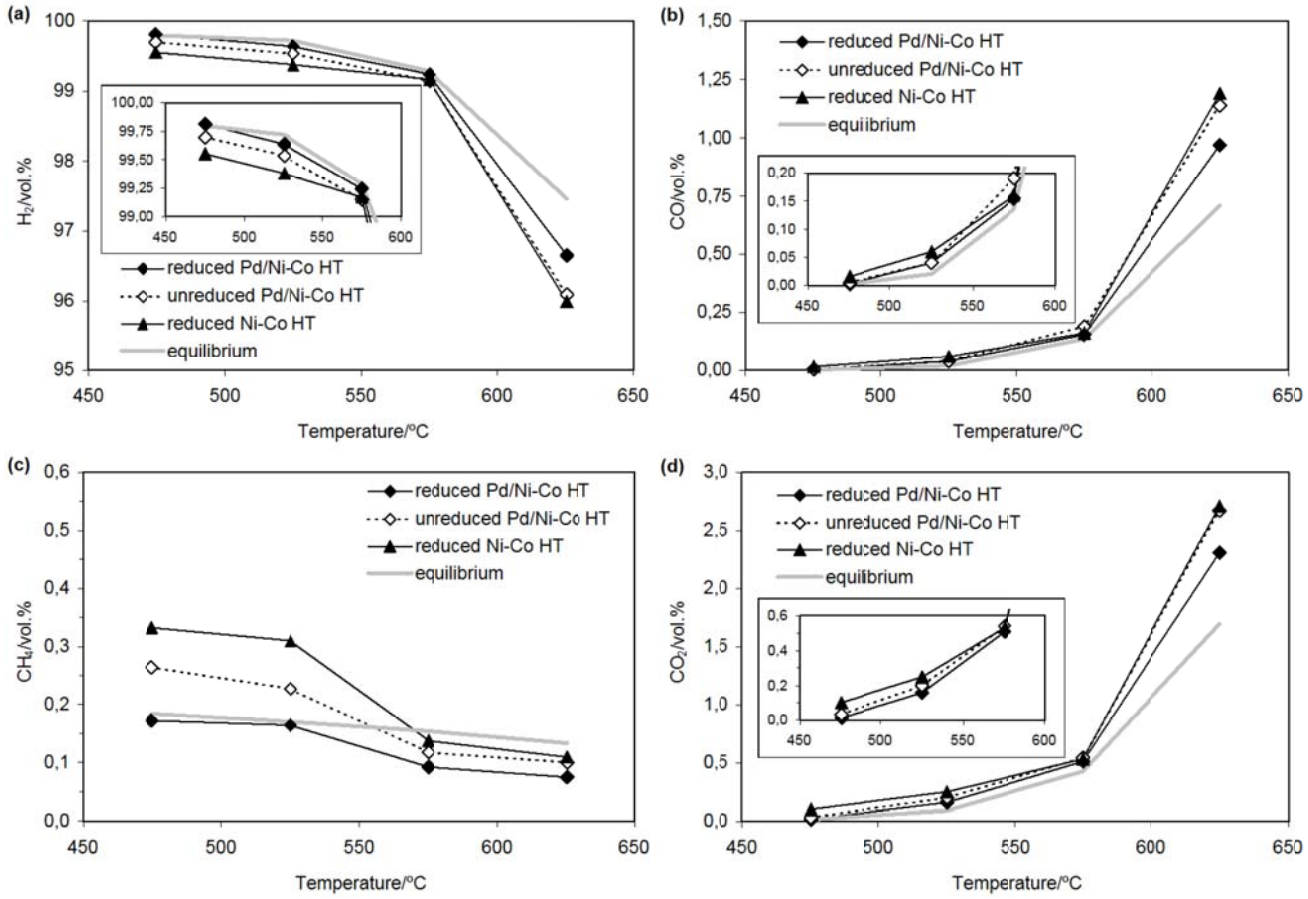

Figure 9. Effect of the reaction temperature on the product gas composition (N_2 free and dry basis) during the SESR process of acetic acid using different catalysts: (a) H_2, (b) CO, (c) CH_4 and (d) CO_2. Reaction conditions: 1 atm; steam/C = 3 mol/mol; WHSV = 0.89 h^{-1}; sorbent to catalyst = 5 g/g and calcined dolomite as sorbent.

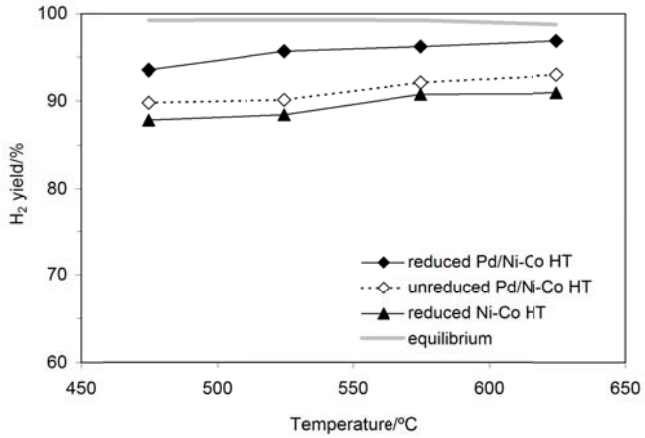

Figure 10. Effect of the reaction temperature on the H_2 yield during the SESR process of acetic acid using different catalysts. Reaction conditions: 1 atm; steam/C = 3 mol/mol; WHSV = 0.89 h^{-1}; sorbent to catalyst = 5 g/g and calcined dolomite as sorbent.

In summary, the SESR of acetic acid at 525 ºC, steam/C of 3 and WHSV of 0.89 h^{-1} using the unreduced Pd/Ni-Co HT catalyst produced a H_2 yield of 90% and a gas which contained 99.5 vol.% of H_2, 0.04 vol.% of CO, 0.23 vol.% of CH_4 and 0.20 vol.% of CO_2. A lower temperature would increase the H_2 content while decreasing the CO and CO_2 concentrations, but a considerable increase in the CH_4 content would be produced, which would reduce the H_2 yield. It has been shown by Fermoso et al.[4b] that an increase in the steam/C ratio used in the SESR process leads to a decrease in the CO and CH_4 concentrations without causing a decrease in the H_2 content and H_2 yield, due to the enhancement of the WGS reaction at high steam/C ratios. These authors also found that a high steam/C ratio favors the conversion of tar and emphasized its importance in SESR processes for obtaining a high H_2 yield. Although a high steam/C ratio may cause the sintering of the catalyst and involves the consumption of larger amounts of energy, this parameter should be analyzed for the present process in future works in order to study the possibility of obtaining higher H_2 yields with a higher degree of H_2 purity. From the thermodynamic analysis of the sorption enhanced steam reforming of acetic acid, Zin et al.[32] showed that operating at a higher steam/C ratio (up to 4.0) resulted in higher H_2 yield and purity at the cost of lower temperature requirements.

Demonstration of SESR coupling with chemical looping and stability of materials

Hydrogen production by SESR of acetic acid coupling with chemical looping was demonstrated by cyclic operation using air for regeneration. The reforming experiments were carried out at 575º C using the unreduced Pd/Ni-Co HT catalyst, while the regeneration in air was done at 770º C. The cycle stability of the catalyst and the CO_2 sorbent in the SESR process was tested in six carbonation/ decarbonation cycles. Figure 11 a shows the H_2 yield, H_2 selectivity and the gas composition (N_2 free and dry basis) during six cycles of SESR with acetic acid. Their values remained quite constant during the six cycles, which indicates no significant deactivation of the catalyst. However, a decrease in the time of the pre-breakthrough stage (Figure 11 b) was observed as the number of cycles proceeded, suggesting a certain change in the kinetics and the CO_2 capture capacity. The CO_2 breakthrough time decreases slightly with increasing cycle number as a result of a loss of the CO_2 capacity of the sorbents. The amount of CO_2 captured was calculated as the difference of the flow rate of CO_2 (g min^{-1}) between the SR and SESR regimes, multiplied by the breakthrough time (min). The CO_2 capture capacity of the dolomite was found to be 0.317 and 0.301 g CO_2/g sorbent during the first and second cycles of reaction, respectively. Dolomite is known to lose its CO_2 capture capacity during multiple cycle operation. Thus, the CO_2 capture capacities, defined as the mass of CO_2 captured per 100 g of calcined dolomite, calculated in these experiments ranged from 31.7 to 22.1% for the cycles one to six. It indicates that the stability of the sorbent material can be considered one of the key challenges in the development of the SESR technology.

In order to understand the mechanisms of the observed deactivation of the sorbent, the characterization of both fresh dolomite and spent catalyst/dolomite mixture were performed. After completion of six cycles of SESR, it was very difficult to separate the catalyst and the sorbent from the catalyst/sorbent mixture. Therefore, XRD and BET surface area measurements of the sorbent/catalyst (5/1 g/g) mixture were obtained. The XRD spectra of both fresh calcined sorbent and spent calcined bed after six cycles of SESR with acetic acid are shown in Figure 12. The XRD patterns both of the fresh sorbent and the spent bed clearly indicate the

presence of CaO and MgO phases. However, the peaks associated to the presence of NiO cannot be distinguished due to heavy overlaps with those corresponding to the MgO phases. The average crystal sizes have been estimated from the XRD peaks using the Scherrer equation and their values are shown in Table 2. The results show a slight increase in the CaO crystal of the sorbent from 32.4 to 35.1 nm after six cycles.

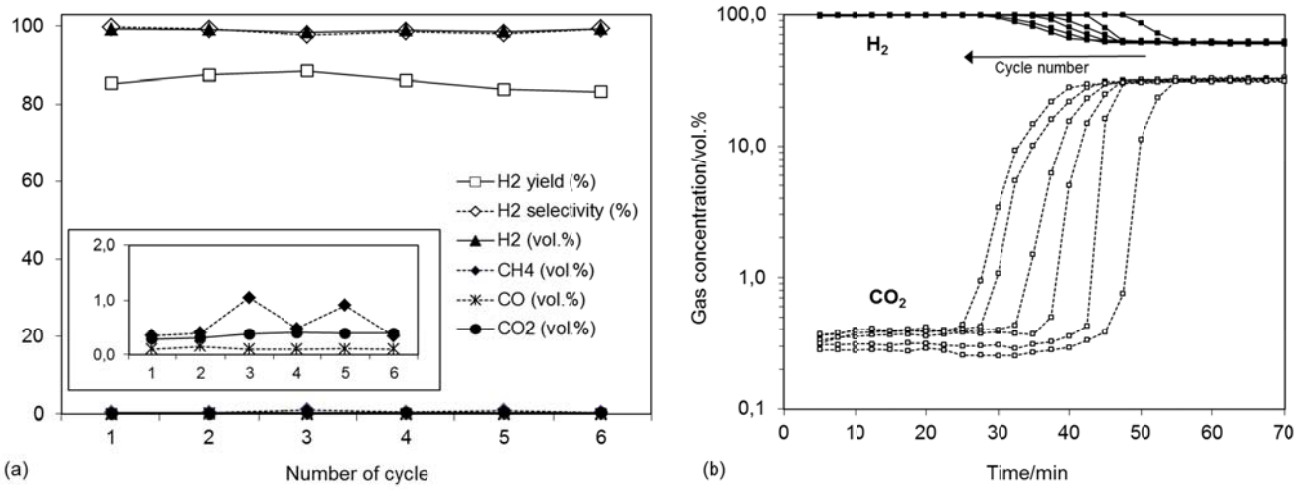

Figure 11. H_2 yield, H_2 selectivity and gas composition during six cycles of SESR with acetic acid. Reaction conditions: 575º C; 1 atm; steam/C = 3 mol/mol; WHSV = 1.786 h^{-1}; sorbent to catalyst = 5 g/g; unreduced Pd/Ni-Co HT catalyst and calcined dolomite as sorbent; regeneration in air at 770º C.

The BET surface area and pore volume of the fresh calcined dolomite were found to be 11.0 $m^2\ g^{-1}$ and 0.16 $cm^3\ g^{-1}$, respectively (Table 2). The initial average surface area of the catalyst/sorbent mixture was calculated to be 33.2 $m^2\ g^{-1}$, whereas it was reduced to 14.2 $m^2\ g^{-1}$ after six cycles (Table 2). Similarly, the pore volume of the mixture was reduced from 0.22 to 0.11 $cm^3\ g^{-1}$ after six cycles of SESR. It means that the surface area of catalysts and sorbents significantly decreased after cycle operation.

Table 2. Physical-chemical properties of both fresh dolomite and spent bed before and after SESR experiments with acetic acid.

Sorbent	BET surface area [$m^2\ g^{-1}$]	BET pore volume [$cm^3 g^{-1}$]	BET pore diameter [nm]	Crystallite size (XRD) [nm]
fresh calcined dolomite	11.0	0.16	59	
CaO				32.4
MgO				26.9
spent calcined bed	14.2	0.11	34	
CaO				35.1
MgO				31.3

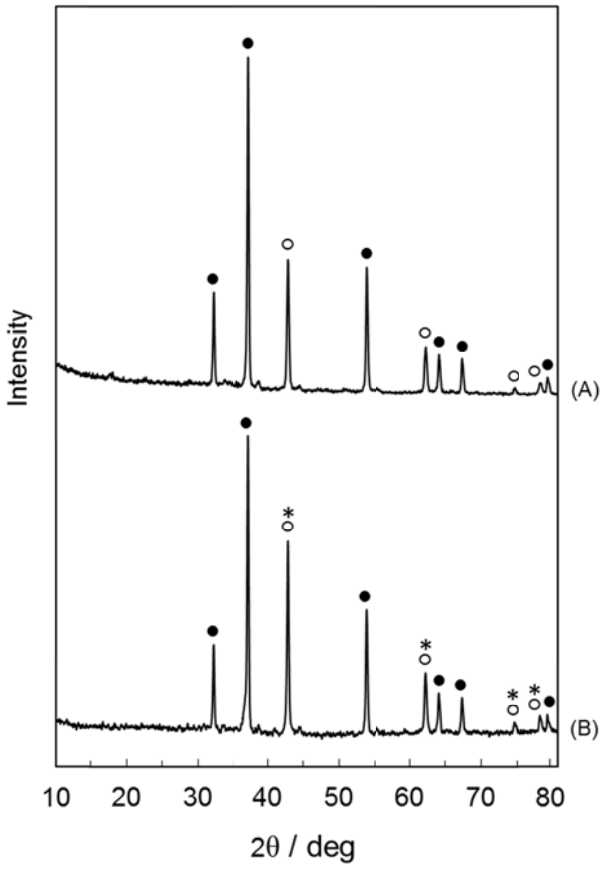

Figure 12. X-ray diffraction (XRD) patterns of fresh calcined dolomite (A) and spent calcined bed (B) after six cycles of SESR with acetic acid. Peaks marked with (●) are characteristic of CaO; peaks marked with (○) are characteristic of MgO; and peaks marked with (*) are characteristic of NiO.

Previously, it has been reported that the surface area of hydrotalcite-derived supports decreased from about 200 m^2 g^{-1} to 20-30 m^2 g^{-1} after more than 50 hours under steam reforming reaction at 630º C and 20 bars, whereas Ni particles were relatively stable[33]. Also, Noor et al.[34] reported a decrease in the surface area of the catalyst/sorbent mixture from 38 m^2 g^{-1} to 12 m^2 g^{-1} after seven cycles of sorption enhanced water gas shift reaction. In addition, the regeneration of the sorbents at high temperature could have caused the sintering of catalysts and sorbents. It should be mentioned that the Ni-Co catalysts were calcined at a relatively low temperature (600 ºC) during their preparation, which was optimized to get a high Ni dispersion but not optimized for the SESR process, where a high temperature (770 ºC) is required for the regeneration of the sorbents. It recommends a high temperature (>750 ºC) for calcination of catalysts in future works. However, since the dolomite had been carbonated during its storage, in the present work the catalyst/sorbent mixture was subjected to an initial regeneration stage at 770 ºC in air before the SESR process. Moreover, taking into account that the contents of H_2, CH_4 and CO during the SESR cycles kept stable, it seems that the decrease in the CO_2 capacity has been mainly result of the deactivation of the sorbent due to the BET surface area decrease and the CaO sintering.

Conclusions

The sorption enhanced steam reforming (SESR) of acetic acid for H_2 production has been performed by using a $CaO/CaCO_3$ cycle for CO_2 capture coupled to a chemical loop of Ni/NiO and Co/Co_3O_4 by means of the use of a novel multifunctional 1%Pd/20%Ni-20%Co HT catalyst. Multifunctional catalysts make it possible to supply heat for sorbent regeneration by oxidizing Ni and Co, and to eliminate the catalyst reduction step between the regeneration and reforming stages in the cycles. The results showed the high activity of the Pd/Ni-Co catalyst in breaking the C-C bond in the SESR of acetic acid. Because of the unique properties of Pd, multifunctional catalysts containing this element make it possible to generate hydrogen after an air regeneration step, which rapidly reduces the Ni and Co oxides. It has been demonstrated that a chemical loop between metal and oxide forms of Ni and Co can occur during the cyclic SESR process, which would make the chemical looping coupled to the sorption enhanced steam reforming process viable. Moreover, the addition of Pd to the catalyst significantly improved the H_2 yield, especially at low space velocities and low temperatures, even when the Pd-promoted catalyst was unreduced, due to a noticeable lower CH_4 content in the produced gas. Nevertheless, H_2 purity was only slightly improved with the addition of Pd. An increase in space velocity and temperature caused a decrease in H_2 purity and an increase in the CO and CO_2 concentrations. The CH_4 content decreased with an increase in temperature or a decrease in the space velocity. The H_2 yield decreased significantly with the space velocity, but it was favored by a rise in temperature. Hydrogen of a high purity (99.5 vol.%) and a high yield (90%) can be obtained from the SESR of acetic acid at 525 ºC, steam/C of 3 and WHSV of 0.89 h^{-1} by using the unreduced 1%Pd/20%Ni-20%Co HT catalyst and calcined dolomite as CO_2 sorbent. The results indicate that the ability of Pd to perform an early reduction of the metal oxide phases contained in the catalyst makes the proposed multifunctional Pd/Ni-Co HT catalyst a promising material for use both as a reforming catalyst and as an oxygen carrier in the assembled SESR-CL cyclic process with acetic acid, allowing a continuous cycling operation in parallel fixed-bed reactors or solid circulating fluidized-bed reactors and contributing to an increase in the energy efficiency of the overall process.

Experimental Section

Feedstock and CO_2 sorbent

Acetic acid was selected as an oxygenated model compound of organic acids contained in the aqueous phase of bio-oils produced by the fast pyrolysis of biomass. Glacial acetic acid was supplied by PANREAC (100% purity). An aqueous solution of acetic acid was prepared with a water-to-acetic acid molar ratio of 6 (steam/C molar ratio of 3). Arctic dolomite, used as a precursor of CaO for the capture of CO_2, was supplied by Franefoss Miljøkalk As, Norway. This has a purity of 98.5 wt.% $CaMg(CO_3)_2$ and no sulfur according to X-ray fluorescence analysis. The dolomite sample was calcined in an air flow at 750 ºC for 4 h prior to its application as CO_2 sorbent. The initial maximum capacity for CO_2 capture was estimated to be 46 wt.%.

Catalyst preparation

The 20%Ni-20%Co hydrotalcite-like material (HT) used as catalyst precursor in the present work (Ni-Co HT) was prepared by co-precipitation of $Ni(NO_3)_2{\cdot}6H_2O$, $Co(NO_3)_3{\cdot}6H_2O$, $Mg(NO_3)_3{\cdot}6H_2O$ and $Al(NO_3)_3{\cdot}9H_2O$. A stoichiometric ratio of cations was chosen so as to yield a 40 wt.% total metal loading of Ni and Co, yielding a

material with the nominal composition of 20%Ni-20%Co. The precipitate obtained was filtered, washed, dried overnight and then calcined at 600 ºC for 6 h. A detailed description of its preparation has been reported elsewhere[24]. The novel 1%Pd/20%Ni-20%Co HT catalyst (Pd/Ni-Co HT) was prepared by the incipient wetness impregnation method. After calcination, the Ni-Co HT precursor was impregnated with a 1% (w/w) loading of Pd. The Pd solution was prepared by dissolving $PdCl_2$ into two equivalents of HCl and diluting them in ethanol to the desired concentration. The sample was then dried for 14 h at 100 ºC and calcined in an air flow at 500 ºC (heating rate of 5 ºC min^{-1}) for 1 h in a muffle oven. The calcined catalyst was pelletized, ground and sieved to the desired particle size (250-500 μm).

The Pd/Ni-Co HT catalyst was reduced and passivated before being characterized by scanning electron microscopy (SEM). The schematic diagram of the experimental setup used to carry out the reduction-passivation process is shown in Figure 13. A catalyst sample was placed in a stainless steel fixed-bed reactor (i.d. 9 mm) and heated at a heating rate of 2 ºC min^{-1} in a mixed flow of H_2 (50 NmL min^{-1}) and N_2 (50 NmL min^{-1}) and then kept at 670 ºC for 10 h. After being cooled down to room temperature under a N_2 atmosphere, the sample was passivated by flowing 1 vol.% of O_2 in N_2 for 1.5 h.

Catalyst characterization

The crystalline structure of the materials was characterized by powder X-ray diffraction (XRD) analysis on a Siemens IFFRACplus-D5005 diffractometer.

Nitrogen physisorption measurements were performed on a Micromeritics Tristar 3000 at -196 ºC. All samples were outgassed overnight under vacuum at 100 ºC before adsorption. The surface area was calculated using the BET equation in the relative pressure interval of 0.01 to 0.30. The adsorption average pore width (4 V/A) was estimated by the Barret-Joyner-Halenda (BJH) method provided by Micromeritics Tristar 3000 built-in software.

Hydrogen chemisorption isotherms were measured on a Micromeritics ASAP 2010C unit at 35 ºC in order to estimate metal dispersion. Samples of freshly calcined catalyst were firstly reduced in 5 vol.% H_2 in a He flow at 670 ºC for 10 h (heating rate 2 ºC min^{-1}) and then evacuated for 0.5 h at 670 ºC and for 1 h at 35 ºC. Then, an adsorption isotherm was recorded at 35 ºC, as in previous studies on Ni-Co bimetallic catalysts[24]. The total hydrogen uptake was used to calculate the dispersion and particle size, given that the HT-derived support material is generally considered unreduced under ambient conditions and the physical adsorption of hydrogen on the support is ignored[33]. The monolayer adsorption capacity was determined by extrapolating the straight-line portion of the total adsorption isotherm to zero pressure. The dispersion (D) of the Pd, Ni and Co metals was calculated, assuming that two metal sites are covered by one hydrogen molecule. Assuming spherical particles, the particle sizes, d(Pd), d(Ni) and d(Co), were calculated from D using the following formulas: d(Pd)(nm) = 116/D(%), d(Ni)(nm) = 101/D(%) and d(Co)(nm) = 96/D(%). For the mixture of Ni and Co, the particle size was averaged by: d(Ni-Co)(nm) = [101/D(Ni)] · (Ni%/100) + [96/D(Co)] · (Co%/100). In the case of the trimetallic catalyst, the particle size was averaged by: d(Pd-Ni-Co)(nm) = [116/D(Pd)] · (Pd%/100) + [101/D(Ni)] · (Ni%/100) + [96/D(Co)] · (Co%/100).

Temperature-programmed reduction (TPR) was performed on a Quantachrome CHEMBET-3000 unit. The experiments were conducted in 7 vol.% of H_2 in Ar (total flow rate of 50 NmL min^{-1}) and at a heating rate of

10 ºC min^{-1} up to 1000 ºC, which was maintained for 30 min. The H_2 consumption was measured by analyzing the effluent gas with a thermal conductivity detector.

Scanning electron microscopy (SEM) analysis was performed on the 1%Pd/20%Ni-20%Co HT catalyst, after reduction and passivation of the sample, in a Quanta FEG 650 scanning electron microscope coupled to an energy dispersive X-ray (EDS) detector for detailed elemental analysis.

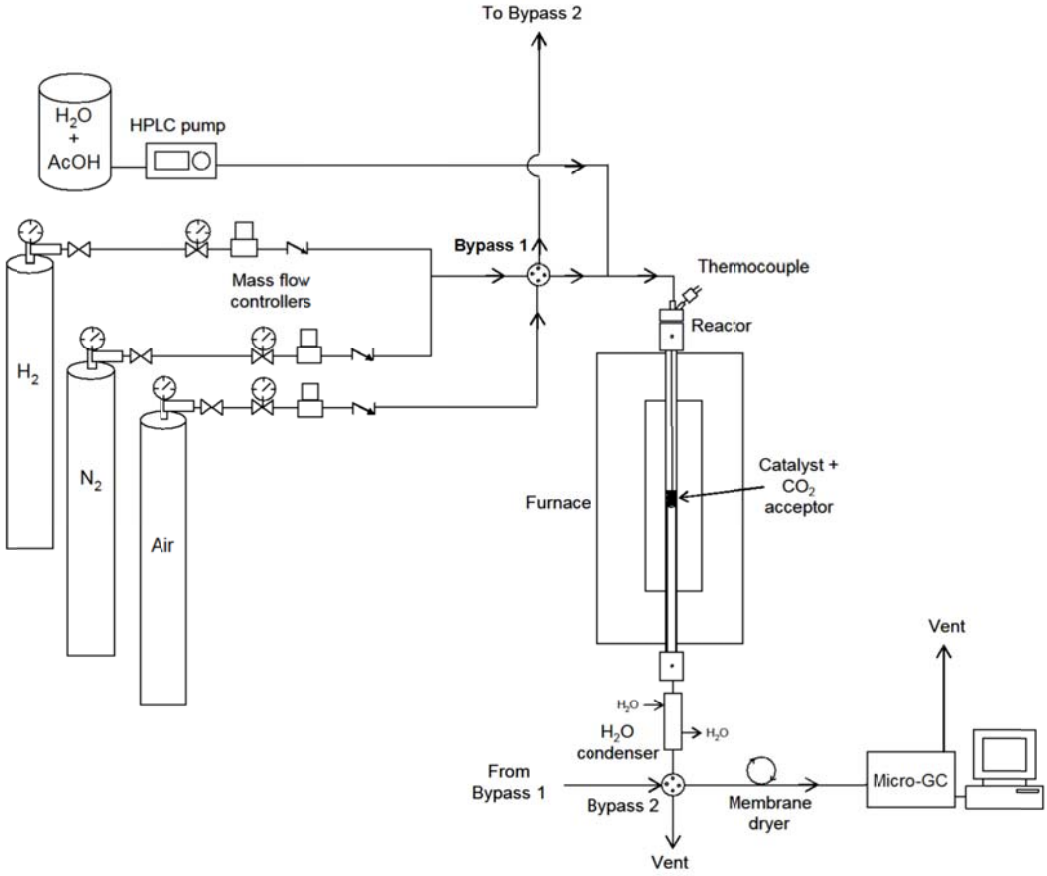

Figure 13. Schematic flow diagram of the experimental setup used for the SESR experiments with acetic acid.

Catalyst testing

The schematic diagram of the experimental setup used for the SESR experiments with acetic acid is shown in Figure 13. It consists of a stainless steel fixed-bed reactor (i.d. 9 mm), which was loaded with a 6 g mixture of calcined dolomite (as CO_2 sorbent) and Ni-Co HT or Pd/Ni-Co HT catalyst, at a sorbent-to-catalyst ratio of 5 g/g. The gases were delivered by Bronkhorst® mass flow controllers, and the aqueous solution of acetic acid was fed in by a Gilson® high-performance liquid chromatography (HPLC) pump. All the experiments were carried out at isothermal (475-625 ºC) conditions and atmospheric pressure. A typical operation procedure was as follows. Fresh catalyst and calcined sorbent materials were used in all the experiments. Since the calcined dolomite was carbonated during its storage, the catalyst and carbonated sorbent mixture were subjected to a regeneration step before the SESR process at 770 ºC in an air flow (200 NmL min^{-1}) until the CO_2 levels dropped to less than 0.5 vol.%. During this process, the catalyst has experienced a thermal treatment at the identical temperatrure of the regeneration. The temperature of 770 ºC was selected from preliminary experiments, taking into account the thermodynamic limitations of the decarbonation reaction and the kinetics of the decarbonation of dolomites[16]. The mixture of regenerated catalyst and sorbent was used directly in the SESR experiments. The regenerated (or oxidized) catalyst is referred to as 'unreduced catalyst' throughout the text. However, in the case of the 'reduced catalyst', the oxidized catalyst was activated by a reduction step after regeneration and before the SESR reactions. The reduction was performed at 670 ºC (heating rate of 2 ºC min^{-1}) under a flowing gas mixture of 50 vol.% H_2/N_2 (total flow rate of 200 NmL min^{-1}) for 10 h. After reduction, the reactor was purged with N_2 and cooled down to the desired reaction temperature. The reaction temperature was measured by a thermocouple inserted into the catalyst/sorbent bed. The liquid reactant mixture (steam/C = 3) was swept by a 50 NmL min^{-1} N_2 flow (used as internal standard), evaporated in an evaporator and then introduced downdraft through the catalyst/sorbent bed at different space velocities (liquid flow rates of 2.5-50 g h^{-1}). The SESR of acetic acid proceeded until the CO_2 sorbent, i.e., calcined dolomite, became saturated and lost its capacity for CO_2 removal. This was followed by conventional steam reforming (SR) and WGS reactions if feeding was maintained.

The effluent gas from the reactor was cooled down by a cooling tank. Moisture was removed by means of a membrane drier. The exiting gas was analyzed using an on-line Agilent® 3000 dual channel Micro GC, equipped with Molsieve and Plot U columns and a TCD detector. The GC was calibrated employing a standard gas mixture at periodic intervals. The detection limit of this equipment for gas analysis was 0.001 vol.%. The species detected were H_2, CH_4, CO and CO_2. The product distribution was calculated on the basis of the dry composition of the gas effluent. The flow rates of the species generated during the experiment were calculated from a nitrogen balance, since the amount of nitrogen fed in and the composition of the nitrogen evolved were known.

In this work, the H_2 yield and H_2 purity were calculated from Equations (10) and (11), respectively:

$$H_2 \text{ yield } (\%) = 100 \cdot (F_{H2}/4 \cdot F_{\text{acetic acid}}) \qquad (10)$$

$$H_2 \text{ purity (vol.\%)} = 100 \cdot (y_{H2}/\Sigma_i\, y_i) \qquad (11)$$

where F_{H2} is the molar flow rate of H_2 produced (mol min^{-1}), $F_{\text{acetic acid}}$ is the molar flow rate of acetic acid fed in (mol min^{-1}), and y_i is the molar content (N_2 free and dry basis) of each species i (H_2, CO, CH_4 and CO_2). The weight hourly space velocity (WHSV) is defined as the ratio of the mass flow rate of the inlet acetic acid to the mass of catalyst ($g_{\text{acetic acid}}\ g_{\text{catalyst}}^{-1}\ h^{-1}$).

Thermodynamic equilibrium calculations

Thermodynamic analysis of the SESR process was conducted under the reaction conditions used in the experimental study. The equilibrium composition was estimated by minimizing the Gibbs free energy. Aspen Plus 7.2 software (Aspentech) was used for the calculations. The RGibbs reactor was specified as the reaction system. The Peng-Robinson property method was used to predict the thermodynamic behaviour of the system. According to the results obtained from the equilibrium prediction under sorption enhanced conditions, the species produced in concentrations higher than 10^{-4} mol% were H_2, CO, CO_2, CH_4, H_2O, CaO and $CaCO_3$. C_2H_6, C_2H_4, C_2H_2 and C (graphite as solid carbon) were also included in the product pool, but their concentrations in the equilibrium stream were null or not high enough to be considered as significant products, as was indicated in previous works[16]. The product mole fractions were calculated on a dry basis.

Acknowledgements

The authors acknowledge financial support from the Research Council of Norway (RCN). They thank Franefoss Miljøkalk A/S (Norway) for supplying Arctic dolomite. J. Fermoso acknowledges funding from the Spanish Ministry of Education, through the National Mobility Program of Human Resources of the National Plan of I-D+i 2008-2011. M.V. Gil acknowledges funding from the CSIC JAE-Doc program, Spain, co-financed by the European Social Fund, and support from the Research Council of Norway through the Yggdrasil program.

***Keywords**: biomass • hydrogen • oxygen carrier • Pd/Ni-Co hydrotalcite catalyst• sorption enhanced steam reforming*

[1] D. B. Levin, R. Chahine, *Int. J. Hydrogen Energy* **2010**, *35*, 4962-4969.

[2] European Commission, Directorate-General for Research/Directorate-General for Energy and Transport, Luxembourg, **2003**, p. 36 pp.

[3] P. C. Hallenbeck, M. Abo-Hashesh, D. Ghosh, *Bioresour. Technol.* **2012**, *110*, 1-9.

[4] a) S. Sato, S.-Y. Lin, Y. Suzuki, H. Hatano, *Fuel* **2003**, *82*, 561-567; b) J. Fermoso, F. Rubiera, D. Chen, *Energy Environ. Sci.* **2012**, *5*, 6358-6367; c) D. Sutton, B. Kelleher, J. R. H. Ross, *Fuel Process. Technol.* **2001**, *73*, 155-173; d) J. Fermoso, B. Arias, M. V. Gil, M. G. Plaza, C. Pevida, J. J. Pis, F. Rubiera, *Bioresour. Technol.* **2010**, *101*, 3230-3235.

[5] a) B. Valle, A. Remiro, A. T. Aguayo, J. Bilbao, A. G. Gayubo, *Int. J. Hydrogen Energy* **2013**, *38*, 1307-1318; b) L. He, J. M. S. Parra, E. A. Blekkan, D. Chen, *Energy Environ. Sci.* **2010**, *3*, 1046-1056; c) K. Shimura, H. Yoshida, *Energy & Environmental Science* **2011**, *4*, 2467-2481.

[6] a) C. Rioche, S. Kulkarni, F. C. Meunier, J. P. Breen, R. Burch, *Appl. Catal. B-Environ.* **2005**, *61*, 130-139; b) J. N. Chheda, G. W. Huber, J. A. Dumesic, *Angew. Chem. Int. Ed.* **2007**, *46*, 7164-7183.

[7] S. Czernik, A. V. Bridgwater, *Energy Fuels* **2004**, *18*, 590-598.

[8] a) J. R. Galdámez, L. García, R. Bilbao, *Energy Fuels* **2005**, *19*, 1133-1142; b) F. Bimbela, D. Chen, J. Ruiz, L. García, J. Arauzo, *Appl. Catal. B-Environ.* **2012**, *119-120*, 1-12.

[9] a) K. Takanabe, K.-i. Aika, K. Seshan, L. Lefferts, *Chem. Eng. J.* **2006**, *120*, 133-137; b) X. Hu, G. Lu, *J. Mol. Catal. A: Chem.* **2007**, *261*, 43-48; c) J. A. Medrano, M. Oliva, J. Ruiz, L. Garcia, J. Arauzo, *Int. J. Hydrogen Energy* **2008**, *33*, 4387-4396.

[10] a) J. Piskorz, D. S. Scott, D. Radlein, in *Pyrolysis Oils from Biomass, Vol. 376*, American Chemical Society, **1988**, pp. 167-178; b) C. A. Mullen, A. A. Boateng, *Energy Fuels* **2008**, *22*, 2104-2109.

[11] a) S. Czernik, R. French, C. Feik, E. Chornet, *Ind. Eng. Chem. Res.* **2002**, *41*, 4209-4215; b) E. C. Vagia, A. A. Lemonidou, *Int. J. Hydrogen Energy* **2007**, *32*, 212-223.

[12] a) M. Rydén, P. Ramos, *Fuel Process. Technol.* **2012**, *96*, 27-36; b) J. R. Fernández, J. C. Abanades, R. Murillo, G. Grasa, *Int. J. Greenh. Gas Control* **2012**, *6*, 126-141; c) V. Dupont, A. B. Ross, I. Hanley, M. V. Twigg, *Int. J. Hydrogen Energy* **2007**, *32*, 67-79; d) J. R. Fernandez, J. C. Abanades, G. Grasa, *Chem. Eng. Sci.* **2012**, *84*, 12-20.

[13] J. C. Abanades, R. Murillo, J. R. Fernandez, G. Grasa, I. Martínez, *Environmental Science & Technology* **2010**, *44*, 6901-6904.

[14] L. He, D. Chen, *ChemSusChem* **2010**, *3*, 1169-1171.

[15] J. Fermoso, L. He, D. Chen, *Int. J. Hydrogen Energy* **2012**, *37*, 14047-14054.

[16] L. He, H. Berntsen, D. Chen, *J. Phys. Chem. A* **2010**, *114*, 3834-3844.

[17] L. He, D. Chen, *ChemSusChem* **2012**, *5*, 587-595.

[18] F. Melo, N. Morlanés, *Catal. Today* **2008**, *133-135*, 374-382.

[19] D. Chen, L. He, *ChemCatChem* **2011**, *3*, 490-511.

[20] M. C. Romano, E. N. Cassotti, P. Chiesa, J. Meyer, J. Mastin, *Energy Procedia* **2011**, *4*, 1125-1132.

[21] F. Cavani, F. Trifirò, A. Vaccari, *Catal. Today* **1991**, *11*, 173-301.

[22] ICDD*, Vol. PDF-2*, International Centre for Diffraction Data, Park Lane Swarthmore, Pennsylvania, USA, **1994**.

[23] M. Bellotto, B. Rebours, O. Clause, J. Lynch, D. Bazin, E. Elkaïm, *The Journal of Physical Chemistry* **1996**, *100*, 8527-8534.

[24] L. He, H. Berntsen, E. Ochoa-Fernández, J. Walmsley, E. Blekkan, D. Chen, *Top. Catal.* **2009**, *52*, 206-217.

[25] E. Ochoa-Fernández, C. Lacalle-Vilà, K. Christensen, J. Walmsley, M. Rønning, A. Holmen, D. Chen, *Top. Catal.* **2007**, *45*, 3-8.

[26] P. Li, C. He, J. Cheng, C. Y. Ma, B. J. Dou, Z. P. Hao, *Appl. Catal. B-Environ.* **2011**, *101*, 570-579.

[27] M. Muñoz, S. Moreno, R. Molina, *Int. J. Hydrogen Energy* **2012**, *37*, 18827-18842.

[28] W. C. Conner, J. L. Falconer, *Chem. Rev.* **1995**, *95*, 759-788.

[29] G. Jacobs, J. A. Chaney, P. M. Patterson, T. K. Das, B. H. Davis, *Applied Catalysis A: General* **2004**, *264*, 203-212.

[30] R. J. Farrauto, M. C. Hobson, T. Kennelly, E. M. Waterman, *Applied Catalysis A: General* **1992**, *81*, 227-237.

[31] R. J. Farrauto, J. K. Lampert, M. C. Hobson, E. M. Waterman, *Appl. Catal. B-Environ.* **1995**, *6*, 263-270.

[32] R. M. Zin, A. Lea-Langton, V. Dupont, M. V. Twigg, *Int. J. Hydrogen Energy* **2012**, *37*, 10627-10638.

[33] L. Chmielarz, P. Kuśtrowski, A. Rafalska-Łasocha, R. Dziembaj, *Thermochim. Acta* **2003**, *395*, 225-236.